PCCP

Accepted Manuscript

ROYAL SOCIETY OF CHEMISTRY

www.rsc.org/pccp

PCCP

COMMUNICATION

Endohedral Ca@B_{38}: stabilization of a B_{38}^{2-} borospherene dianion by metal-encapsulation†

eceived 00th January 20xx,
Accepted 00th January 20xx

DOI: 10.1039/x0xx00000x

www.rsc.org/

Qiang Chen,[ab] Hai-Ru Li,[b] Chang-Qing Miao,[a] Ying-Jin Wang,[ab] Hai-Gang Lu,[b] Yue-Wen Mu,[b] Guang-Ming Ren,*[a] Hua-Jin Zhai,*[bc] and Si-Dian Li*[b]

Based on extensive global-minimum searches and first-principles electronic structure calculations, we present the viability of an endohedral metalloborospherene C_s Ca@B_{38} (1) which contains a C_s B_{38}^{2-} (2) dianion composed of interwoven boron double chains with a σ+π double delocalization bonding pattern, extending the B_n^q ($q = n-40$) borospherene family from $n = 39-42$ to $n = 38$. Transition metal endohedral complexes C_s M@B_{38} (M = Sc, Y, Ti) (3, 5, 7) based on C_s B_{38}^{2-} (2) are also predicted.

As an electron-deficient element, boron has a strong propensity to form polyhedral structures with multicenter chemical bonding. However, gas-phase $B_n^{-/0}$ clusters have proved to be planar or quasi-planar in a wide range of sizes (n = 3–25, 27, 30, 35, 36),[1–10] in stark contrast to bulk boron. The possibility of all-boron fullerenes was not considered prior to the 2007 proposal of B_{80} fullerene,[11] which is constructed from C_{60} by capping the 20 surface hexagons. Subsequent computational investigations, however, showed that B_{80} strongly favors the core-shell-type structures.[12,13] The first all-boron fullerenes D_{2d} B_{40}^- and B_{40}, referred to as borospherenes in literature, were discovered in 2014 by Zhai *et al.* in a combined experimental and theoretical study.[14] The first axially chiral borospherenes C_3/C_2 B_{39}^- were observed by Chen *et al*. in 2015.[15] Two cationic chiral members C_1 B_{41}^+ and C_2 B_{42}^{2+} were recently introduced to the borospherene family by Chen *et al*. on the basis of global minimum (GM) structural searches.[16] The borospherenes B_{39}^-, B_{40}, B_{41}^+, and B_{42}^{2+} reported so far form a π-isovalent B_n^q series in different charge states ($q = n-40$). They are all composed of twelve interwoven boron double-chains (BDCs) with six hexagonal or heptagonal faces, that is, $n_6 + n_7 = 6$ with (n_6, n_7) = (3, 3), (2, 4), (1, 5), and (0, 6) for n=39, 40, 41, and 42, respectively. Such "cubic-box-like" borospherenes can be viewed as boron analogues of cubane (C_8H_8).[14–16] These borospherenes possess a universal bonding pattern of σ+π double delocalization, with 12 multicenter two-electron (mc-2e) π-bonds over a σ-skeleton with (n + 8) three-center two-electron (3c-2e) σ-bonds.[14–16]

The observations of D_{2d} $B_{40}^{-/0}$ and C_3/C_2 B_{39}^- lead to a surge of research activities in borospherene chemistry, which is expected to parallel that of the fullerenes. Endohedral metalloborospherenes M@B_{40} (M = Ca, Sr) were firstly predicted by Bai *et al.* at the density functional theory (DFT) level.[17] A computational study on the electronic structure and electronic spectra of D_{2d} B_{40},[18] a topological analysis of D_{2d} B_{40},[19] a theoretical study on endohedral M@B_{40} (M = Sc, Y, La),[20] a molecular dynamics study on D_{2d} B_{40} "nanobubble" at high temperatures (1000 and 1200 K),[21] a theoretical prediction of the hydrogen-storage capacity of B_{40},[22] and a computational design of Au-B_{40}-Au rectifier and photodetector[23] quickly followed. Very recently, Chen *et al.* predicted the first axially chiral endohedral Ca@B_{39}^+ monocation, in which the B_{39} cage serves as a superhalogen.[24] Borospherenes (B_{39}^-, B_{40}, B_{41}^+, and B_{42}^{2+}) possess the suitable cavities with a diameter of about 6.0 Å, which can host various kinds of alkaline earth and transition metals to form stable endohedral metalloborosphererenes, similar to the well-known endohedral metallofullerenes: M@C_{60} (M = La, Ca) and M@C_{76} (M = Ca, Sr, Sm, Yb).[25–32] Borospherenes are also capable of forming stable exohedral metalloboroppherenes on the surface heptagons, such as the recently predicted M&B_{40} (M = Be, Mg).[17] Concerning smaller fullerene-like boron clusters, a high-symmetry D_{2h} B_{38} cage was recently predicted to be the lowest-lying isomer at the DFT level.[33,34] Based on D_{2h} B_{38}, a series of endohedral complexes M@B_{38} (M = Sc, Y, Ti) were subsequently proposed by encapsulating a transition metal atom inside the D_{2h} B_{38} cage.[35] Note that the D_{2h} B_{38} cage possesses four hexagon holes, as well as two capped hexagons. This structural pattern is basically different from the B_n^q borospherene series (B_{39}^-, B_{40}, B_{41}^+, and B_{42}^{2+}) which are composed of interwoven BDCs with six hexagon/heptagon holes (but without capped hexagons).[14,15] Moreover, endohedral M@B_{40} (M = Ca, Sr) and M@B_{38} (M = Sc, Y, Ti) clusters involve electron donation from the metal centers to the high-lying LUMOs of D_{2d} B_{40} and D_{2h} B_{38} cages which have huge HOMO – LUMO gaps.[14,33] Such orbital occupations should destabilize the endohedral systems thermodynamically. On the other hand, for neutral B_n cages with n < 40 which lack the necessary valence electrons to match the σ+π double delocalization bonding pattern for stable borospherenes,

[a] Institute of Materials Science and Department of Chemistry, Xinzhou Teachers' University, Xinzhou 034000, China. E-mail: rgm_xztc@126.com
[b] Nanocluster Laboratory, Institute of Molecular Science, Shanxi University, Taiyuan 030006, China. E-mail: hj.zhai@sxu.edu.cn, lisidian@sxu.edu.cn
[c] State Key Laboratory of Quantum Optics and Quantum Optics Devices, Shanxi University, Taiyuan 030006, China

† Electronic Supplementary Information (ESI) available. See DOI: 10.1039/x0xx00000x

metal encapsulation is anticipated to help stabilize the systems. The current work represents an exploration in this direction.

Based on extensive GM searches and first-principles calculations, we present herein the possibility of the neutral endohedral C_s Ca@B_{38} (**1**) which is composed of twelve interwoven BDCs with a σ+π double delocalization bonding pattern. Ca@B_{38} (**1**) is a charge-transfer complex Ca^{2+}@B_{38}^{2-} which contains a C_s B_{38}^{2-} (**2**) borospherene dianion effectively stabilized by a Ca^{2+} cation encapsulated inside. The infrared (IR) and Raman spectra of **1**, as well as the photoelectron spectra of two C_s Ca@B_{38}^- monoanions corresponding to the two lowest-lying isomers of CaB_{38} are simulated, which should facilitate their forthcoming experimental characterizations. Transition metal endohedral C_s M@B_{38} (M = Sc, Y, and Ti) based on C_s B_{38}^{2-} (**2**) are also predicted which turn out to be far more stable than the recently proposed C_{2v} M@B_{38} endohedral clusters[35] based on D_{2h} B_{38}.[33-34]

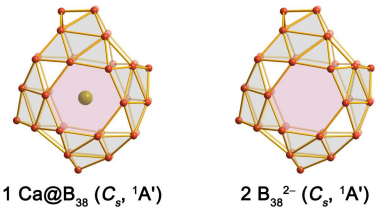

Fig. 1 Optimized strucuture of C_s Ca@B_{38} (**1**) compared with that of C_s B_{38}^{2-} (**2**) at PBE0/6-311+G(d) level. The eight almost perfectly planar, close-packed B_6 triangles at the corners of the cubic-box are shaded in grey.

Global structural searches were performed for CaB_{38} using the Minima Hopping (MH) algorithm[13,36] at DFT, in combination with manual structural constructions based on typical planar, cage-like, and tubular isomers of B_{38}.[33,34,37] Low-lying isomers were then fully optimized with frequencies checked and their relative energies evaluated at the hybrid DFT-PBE0[38] level with the 6-311+G(d) basis set[39] as implemented in the Gaussian 09 suite.[40] The Stuttgart relativistic small-core pseudopotential and valence basis sets[41,42] were used for Sr and Y. Relative stabilities of the low-lying isomers within 0.5 eV were further refined using the coupled cluster method with triple excitations (CCSD(T))[43–45] implemented in MOLPRO[46] with the 6-311G(d) basis set at PBE0 geometries. Molecular dynamics (MD) simulations were performed for the two lowest-lying isomers of CaB_{38} at 200, 300, and 500 K for 30 ps using the CP2K suite.[47] The optimized endohedral Ca@B_{38} (**1**) is depicted in Fig. 1, compared with that of the B_{38}^{2-} (**2**) dianion. Alternative isomeric structures are summarized in Fig. S1 for CaB_{38} in the Electronic Supplementary Information (ESI†). Figure 2 shows the configuration energy spectrum of CaB_{38} at PBE0. Figure 3 presents the bonding patterns of the two lowest-lying isomers of Ca@B_{38} using the adaptive natural density partitioning (AdNDP) method,[48] which includes the mc-2e bonding elements. Figure 4 depicts the simulated photoelectron spectra of two C_s Ca@B_{38}^- monoanions which correspond to the two lowest-lying isomers of CaB_{38} (Fig. 2), using the time-dependent DFT (TD-PBE0) approach.[49] Fig. 5 shows the optimized structures of endohedral C_s M@B_{38} (M = Sc, Y, and Ti) (**3**, **5**, **7**), compared with their C_{2v} M@B_{38} counterparts (**4**, **6**, **8**).

Considering the fact that high-symmetry cage-like D_{2h} B_{38} has been predicted to be the lowest-energy isomer of B_{38} at PBE0,[33] it is reasonable to anticipate that the endohedral D_{2h} Ca@B_{38} cluster be energetically favorable for CaB_{38}. However, as clearly indicated in Fig. S1 in the ESI†, our MH global searches, with more than 2,800 stationary points being probed on the potential energy surface, show that a dramatic structural change occurs from B_{38} to CaB_{38}: the endohedral C_s Ca@B_{38} (**1**, ^{1}A') turns out to be the GM of CaB_{38} complex, which possesses a C_s B_{38} cage composed of twelve interwoven BDCs with four hexagonal and two heptagonal faces, that is, (n_6, n_7) = (4, 2). In contrast, the endohedral D_{2h} Ca@B_{38} based on the D_{2h} Ca@B_{38} cage motif is much less stable (by 1.47 eV; Fig. S1 in the ESI†) than the GM, mainly due to the fact that it involves an electron transfer from the Ca center to the high-lying LUMO (2.25 eV above the HOMO) of the D_{2h} B_{38} cage.[33]

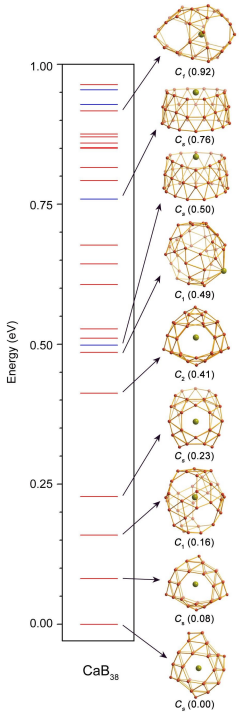

Fig. 2 Configurational energy spectrum of CaB_{38} at PBE0/6-311+G(d), with the relative energies indicated in eV. The red and blue bars denote cage-like structures and triple-ring tubes, respectively.

Interestingly, C_s Ca@B_{38} (**1**) possesses a C_s B_{38} cage motif which follows the structural pattern of the borospherene family. The C_s B_{38} cage can be obtained by replacing two neighboring B_7 heptagons on the waist of D_{2d} B_{40} with two B_6 hexagons,[14] or by replacing two neighboring hexagons on cage-like C_{2h} B_{36} with two heptagons,[9] followed by a full structural optimization. Ca@B_{38} (**1**) looks like a filled "basket", with two staggered heptagons on the top, two eclipsed hexagons in the middle, and two staggered hexagons at the bottom. It can also be viewed as a distorted cubic-box made of eight almost perfectly planar, close-packed B_6 triangles at the eight corners (Fig. 1), similar to D_{2d} B_{40}.[14] With 46 B_3 triangles, four B_6 hexagons, and two B_7 heptagons on surface, Ca@B_{38} (**1**) follows the Euler's rule: E (88 edges) = F (46 triangular + 4 hexagonal + 2 heptagonal faces) + V (38 vertices) − 2. As detailed

below, **1** is a charge-transfer complex in nature, $Ca^{2+}@B_{38}^{2-}$, which follows the universal bonding pattern of σ+π double delocalization for stable borospherenes. Here the B_{38}^{2-} dianion cage is effectively stabilized by the Ca^{2+} dication encapsulated inside, mainly via electrostatic effect. Ca@B_{38} (**1**) represents the first neutral endohedral metalloborospherene with a C_s B_{38}^{2-} shell (**2**).

The second lowest-lying isomer C_s Ca@B_{38} (^{1}A'), which contains three hexagons and three heptagons ((n_6, n_7) = (3, 3)), lies very close in energy to the GM (by 0.08 eV at PBE0; Fig. 2). It possesses a C_s B_{38} cage that can be achieved by replacing one B_7 heptagon on D_{2d} B_{40} with a B_6 hexagon and removing one B atom from a BDC to form a tetracoordinate B "defect" site between two neighboring hexagons on the mirror surface, similar to the experimentally observed C_2 B_{39}^-.[15] At the more accurate CCSD(T) level, the relative energy between these two isomers is only 0.03 eV, indicating that they are practically isoenergetic isomers and may coexist in experiments.

The third lowest-lying isomer C_1 Ca@B_{38} (^{1}A) is 0.16 eV above the GM at PBE0. It also contains three hexagons and three heptagons, that is, (n_6, n_7) = (3, 3), which can be obtained from the experimentally observed C_3 B_{39}^- [15] by removing one B atom from a BDC between two neighboring heptagons to form a tetracoordinate B site. The fourth isomer C_s Ca@B_{38} (^{1}A) lies 0.23 eV higher than the GM, with two neighboring hexagons and four heptagons ((n_6, n_7) = (2, 4)). It can be achieved by replacing one hexagon from C_3 B_{39}^- [15] with a heptagon, with one heptagon on the mirror surface possessing two tetracoordinate B sites on opposite sides. The fifth isomer C_2 Ca@B_{38} (^{1}A) lies 0.41 eV above the GM. It also possesses two hexagons and four heptagons ((n_6, n_7) = (2, 4)), with two tetracoordinate B sites at the two ends of the C_2 axis. The sixth isomer C_1 Ca&B_{38} (^{1}A) with a relative energy of 0.49 eV is the first exohedral isomer, with the Ca atom capping a B_9 ring. The seventh isomer C_s Ca©B_{38} (^{1}A') is a capped triple-ring tube, being 0.50 eV higher than the GM. At the more reliable CCSD(T) level, the third to seventh isomers are 0.06, 0.09, 0.18, 0.22, and 0.40 eV higher than the GM, respectively, well supporting the energetics at PBE0. The first quasi-planar C_s CaB_{38} (^{1}A') with a Ca-capped B_8 octagon lies 1.36 eV higher than the GM at PBE0 (Fig. S1 in the ESI†). Note that the five lowest-lying isomers of CaB_{38} all possess endohedral geometries which are the most possible candidates to be synthesized in experiments. Preliminary investigations at PBE0 also indicate that both endohedral C_s Mg@B_{38} and C_s Sr@B_{38} based on C_s B_{38}^{2-} (**2**) are true minim of the systems, with the former favoring an exohedral C_1 Mg&B_{38} (similar to the sixth isomer of CaB_{38} in Fig. 2) by 0.75 eV and the latter favoring a capped triple-ring tubular C_s Sr©B_{38} (similar to the seventh isomer of CaB_{38}) by 0.12 eV, respectively, possibly due to size effect in the alkaline earth metal series.[17]

The stabilities of the two lowest-lying CaB_{38} isomers are further explored using the MD simulations. As shown in Fig. S2 in the ESI†, Ca@B_{38} (**1**) is dynamically stable at 200, 300, and 500 K, with the root-mean-square-deviations of RMSD = 0.06, 0.07, and 0.10 Å and maximum bond length deviations of MAXD = 0.20, 0.24, and 0.36 Å (on average), respectively (Fig. S2a). The second C_s isomer is also stable at both 200 and 300 K with RMSD = 0.06 and 0.08 Å and MAXD = 0.22 and 0.27 Å, respectively. However, it starts to fluctuate between two equivalent C_s isomers at 500 K with RMSD = 0.13 Å and MAXD = 0.56 Å (Fig. S2b). Interestingly, the two C_s isomers are interlinked *via* a C_2 intermediate structure in a concerted mechanism, which contains a tetracoordinate B site between two neighboring heptagons on C_2 axis (Fig. S2c). Further simulations indicate that Ca@B_{38} (**1**) also "hops" at 700 K between the three lowest-lying isomers of CaB_{38} (Fig. 2). The MD behaviors reflect the glassy nature of nanoboron at high temperatures.[15,16,21,24]

Endohedral metalloborospherenes C_s Ca@B_{38} (**1**) and the second lowest-lying C_s Ca@B_{38} possess unique electronic structures and bonding patterns. Indeed, they have the large HOMO–LUMO gaps of 2.70 eV and 2.58 eV at PBE0 (Fig. S3), respectively, comparable with the corresponding values of 2.89, 2.73, and 3.13 eV obtained for C_3 B_{39}^-, C_2 B_{39}^-, and D_{2d} B_{40} at the same level.[14,15] Natural bonding orbital (NBO) analyses show that the Ca centers in these complexes carry the positive charges of +1.69 |e| and 1.71 |e|, respectively, with the electronic configurations of [Ar]$4s^{0.12}3d^{0.17}$ and [Ar]$4s^{0.12}3d^{0.16}$. These results clearly indicate that the Ca center in these complexes donates two $4s^2$ electrons to the C_s B_{38} cage which behaves like a superoxygen (similar to B_{39} which serves as a superhalogen in Ca@B_{39}^+ [24]). These charge-transfer complexes mainly exhibit ionic interactions between the Ca^{2+} dication center and the B_{38}^{2-} dianion shell. Weak back donations from the π orbitals of B_{38}^{2-} (as analyzed below) to the empty *4d* orbitals of Ca may also contribute to the stabilization of the complexes. The calculated formation energies of ΔE_f = −127.7 and ΔE_f = −131.9 kcal/mol with respect to B_{38}(C_s) + Ca = Ca@B_{38}(C_s) and the vertical ionization potentials of 7.35 and 7.16 eV further demonstrate the thermodynamic stability of these neutral complexes.

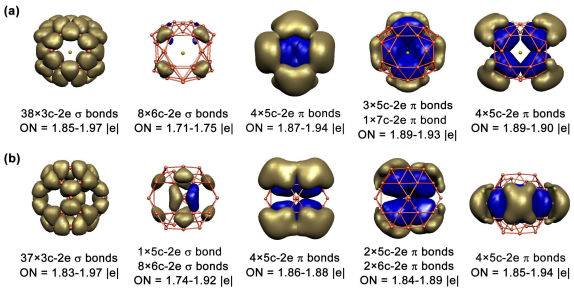

Fig. 3 The AdNDP bonding patterns of (a) the global minimum CaB_{38} (**1**) and (b) the second lowest-lying isomer CaB_{38}, with the occupation numbers (ONs) indicated. Both strucutres are rotated with respect to the oroginal orientations in Fig. 1 and Fig. 2 to make their mirror planes perpendicular to the paper surface.

The AdNDP analyses reveal the bonding pattern of complex C_s CaB_{38} (**1**) and its second lowest-lying isomer. As shown in Fig. 3a, **1** possesses 38 3c-2e σ bonds on 38 B_3 triangles, as well as 8 6c-2eσ bonds on 8 B_6 triangles on the cage surface. Since the central B_3 triangles make major contribution to the 6c-2e σ bonds, the σ framework can be practically treated as 46 3c-2e σ bonds, evenly distributed on the cage surface with one σ bond per B_3 triangle. The remaining 12 bonds form the π framework. It can be classified into three groups, with one 7c-2e π bond over the BDC between two neighboring heptagons and 11 5c-2e π bonds over the other 11 BDCs, which again cover the cage surface almost uniformly. Thus all 116 valence electrons in **1** participate in delocalized σ and π covalent bonds on the cage surface, following the established

bonding pattern of σ+π double delocalization for borospherenes.[14−16] The second lowest-lying endohedral isomer C_s Ca@B_{38} also features a similar bonding pattern, with 45 3c-2e σ bonds on B_3 triangles and one 5c-2e σ bond at the tetracoordinate B site, as well as 12 5c-2e or 6c-2e π bonds (Fig. 3b). There exist no localized bonds in these complexes.

Note that a neutral C_s B_{38} cage lacks two valance electrons to satisfy the σ+π double delocalization bonding requirement of a borospherene; the Ca center in **1** donates exactly two $4s^2$ electrons to compensate for this electron deficiency. The optimized C_s B_{38}^{2-} dianion (**2**) is a true minimum with the smallest vibrational frequency of 160 cm^{-1} and the HOMO–LUMO energy gap of 2.54 eV. It possesses exactly the same σ+π double delocalization bonding pattern as C_s CaB_{38} (**1**) (Fig. 3a). It is also 3D aromatic with the highly negative nucleus-independent chemical shift (NICS)[50] of −37 ppm at the cage center, comparable to the corresponding value of NICS=−42 ppm of D_{2d} B_{40}.[14] However, C_s B_{38}^{2-} (**2**) is not the GM of the dianion due to strong intramolecular Coulomb repulsion in the cage structure. The Ca center in **1** serves as a dication that neutralizes the negative charge the B_{38}^{2-} dianion cage carries, rendering high stability to **1** as the GM of the complex. Similar analyses apply to the second lowest-lying isomer of CaB_{38} in Fig. 2.

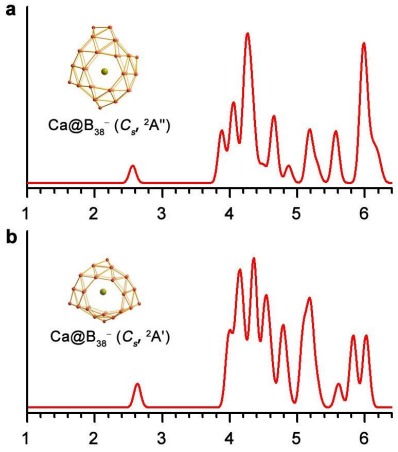

Fig. 4 Simulated photoelectron spectra of (a) C_s Ca@B_{38}^- (**1**) and (b) C_s Ca@B_{38}^- which correspond to the global minimum and the second lowest-lying isomer of CaB_{38} shown in Fig. 2, respectively.

Anion photoelectron spectroscopy in combination with first-principles calculations has proved to be a powerful approach in characterizing nanoclusters in the gas phase.[1−10,14,15] We simulate the photoelectron spectra of the two C_s Ca@B_{38}^- monoanions which correspond to the two lowest-lying isomers of CaB_{38} at PBE0 (Fig. 4) to aid their future experimental characterizations. Remarkably, the two isomers possess similar photoelectron spectra with the experimentally observed D_{2d} B_{40}^-.[14] The calculated first adiabatic and vertical detachment energies (ADE/VDE) of the two C_s Ca@B_{38}^- isomers are 2.44/2.55 and 2.52/2.62 eV, respectively. Their calculated energy gaps amount to 1.32 and 1.35 eV. The sizable energy gaps of the two C_s Ca@B_{38}^- monoanions are consistent with the electronic stability of their neutrals which have large HOMO-LUMO gaps as presented above (Fig. S3). In fact, C_s Ca@B_{38} (**1**) and the second lowest-lying C_s Ca@B_{38} are both π-isovalent with the observed D_{2d} B_{40} borospherene. These neutral metalloborospherenes and their monoanions invite forthcoming experimental explorations.

Vibrational spectroscopy has also proved to be an effective approach for experimental studies of nanoclusters.[51] We calculate the vibrational frequencies and simulate the IR and Raman spectra of Ca@B_{38} (**1**) at PBE0 (Fig. S4 in the ESI†), which are compared with those of B_{38}^{2-} (**2**). The three major IR peaks at 1220 (a'), 811 (a'), and 416 (a") in **2** are basically maintained in **1**, with small blue shifts (Fig. S4a). The main Raman features of **2** are also inherited in **1** (Fig. S4b). The two a' breathing modes at 254 cm^{-1} and 454 cm^{-1} belong to "radial breathing modes" (RBMs) of the B_{38}^{2-} (**2**) cage. RBMs have been used to identify the hollow structures of the single-walled boron nanotubes.[52]

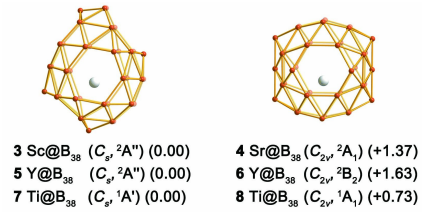

Fig. 5 Optimized endohedral C_s M@B_{38} (M = Sc, Y, Ti) (**3**, **5**, and **7**) compared with the recently proposed C_{2v} M@B_{38} (M = Sc, Y, Ti) (**4, 6,** and **8**), with their relative energies indicated in eV at PBE0 level. High symmetry structures are depicted for comparison and clarity.

Lastly, we brief the results obtained for the series of transition metal doped endohedral complexes: M@B_{38} (M = Sc, Y, Ti). As shown in Fig. 5, the endohedral C_s Sc@B_{38} (**3**), C_s Y@B_{38} (**5**), and C_s Ti@B_{38} (**7**) based on the C_s B_{38}^{2-} (**2**) motif are 1.37, 1.63, and 0.73 eV more stable than the recently proposed C_{2v} Sc@B_{38} (**4**), C_{2v} Y@B_{38} (**6**), and C_{2v} Ti@B_{38} (**8**) [35] based on the D_{2h} B_{38} cage [33] at PBE0 level, respectively. Such huge energy differences are well in agreement with the calculated encapsulation energies of -163.5, -114.5, -182.8, -127.8, -186.9, and -152.7 kcal/mol for **3**, **4**, **5**, **6**, **7**, and **8**, respectively, and strongly suggest that **3**, **5**, and **7** be far more viable in experiments than **4**, **6**, and **8**. NBO analyses show that the metal centers in **3**, **4**, **5**, **6**, **7**, and **8** possess the natural atomic charges of +1.09, +0.80, +1.07, +1.15, +0.88, and +0.50 |e|, respectively, indicating that the transition metal centers donate valence electrons to the cage-like B_{38} ligands, in line with the fact that boron has a higher electronegativity (2.04 in Pauling scale) than all the transition metals Sc (1.36), Y (1.22), and Ti (1.54) concerned in this work. The high stabilities of **3**, **5**, and **7** over **4**, **6**, and **8** can be understood based on the fact that the cage-like C_s B_{38} ligand requires extra electrons from the metal center to satisfy the bonding pattern of a stable borospherene while D_{2h} B_{38} possesses a stable closed-shell electronic configuration with a huge HOMO–LUMO gap of 2.25 eV. [33] There exist also obvious π→d back donations from the B_{38} ligands to the transition metal centers in these complexes, as demonstrated by the electron configurations of Sc [Ar]$4s^{0.16}3d^{1.75}$, Y [Kr]$5s^{0.20}4d^{1.30}$), and Ti [Ar]$4s^{0.15}3d^{2.97}$ in **3**, **5**, and **7**, respectively. We stress here that the current prediction of **3**, **5**, and **7** testifies to the idea of computational design of novel boron nanostructures on the basis of the structural principles and bonding patterns of borospherenes.

In conclusion, we have presented the viability of the endohedral metalloborospherene Ca@B_{38} (**1**) via extensive global structural searches, first-principles calculations, and bonding analyses. Ca@B_{38} (**1**) contains a B_{38}^{2-} (**2**) borospherene shell, which is stabilized by the

encapsulation of a Ca^{2+} center, forming the charge-transfer complex $Ca^{2+}@B_{38}^{2-}$. The complex is composed of twelve interwoven BDCs with six hexagonal/heptagonal faces and satisfy the bonding pattern of σ+π double delocalization for borospherenes. Similar transition-metal-doped endohedral metalloborospherenes C_s M@B_{38} (**3**, **5**, **7**) are also predicted computationally, which turn out to be far more stable than the previously proposed C_{2v} M@B_{38} clusters (**4**, **6**, **8**). The results achieved in this work suggest vast opportunities for rational design of novel boron nanostructures using the structural and bonding patterns of borospherenes.

Acknowledgements

This work was supported by the National Natural Science Foundation of China (21373130, 21573138), the Key Research Project of Xinzhou Teachers' University (XK201303), and the State Key Laboratory of Quantum Optics and Quantum Optics Devices (KF201402). H.J.Z. gratefully acknowledges the start-up fund from Shanxi University for support.

Notes and references

1 H. J. Zhai, A. N. Alexandrova, K. A. Birch, A. I. Boldyrev and L. S. Wang, *Angew. Chem. Int. Ed.,* 2003, **42,** 6004–6008.
2 H. J. Zhai, B. Kiran, J. Li and L. S. Wang, *Nat. Mater.,* 2003, **2,** 827–833.
3 B. Kiran, S. Bulusu, H. J. Zhai, S. Yoo, X. C. Zeng and L. S. Wang, *Proc. Natl. Acad. Sci. U. S. A.,* 2005, **102,** 961–964.
4 W. Huang, A. P. Sergeeva, H. J. Zhai, B. B. Averkiev, L. S. Wang and A. I. Boldyrev, *Nat. Chem.,* 2010, **2,** 202–206.
5 E. Oger, N. R. M. Crawford, R. Kelting, P. Weis, M. M. Kappes and R. Ahlrichs, *Angew. Chem. Int. Ed.,* 2007, **46,** 8503–8506.
6 W. L. Li, Y. F. Zhao, H. S. Hu, J. Li and L. S. Wang, *Angew. Chem. Int. Ed.,* 2014, **53,** 5540–5545.
7 W. L. Li, Q. Chen, W. J. Tian, H. Bai, Y. F. Zhao, H. S. Hu, J. Li, H. J. Zhai, S. D. Li and L. S. Wang, *J. Am. Chem. Soc.,* 2014, **136,** 12257–12260.
8 Z. A. Piazza, H. S. Hu, W. L. Li, Y. F. Zhao, J. Li and L. S. Wang, *Nat. Commun.,* 2014, **5,** 3113.
9 Q. Chen, G. F. Wei, W. J. Tian, H. Bai, Z. P. Liu, H. J. Zhai and S. D. Li, *Phys. Chem. Chem. Phys.,* 2014, **16,** 18282–18287.
10 (a) A. N. Alexandrova, A. I. Boldyrev, H. J. Zhai and L. S. Wang, *Coord. Chem. Rev.,* 2006, **250,** 2811-2866; (b) C. Romanescu, T. R. Galeev, W. L. Li, A. I. Boldyrev and L. S. Wang, *Acc. Chem. Res.,* 2013, **46,** 350-358; (c) A. P. Sergeeva, I. A. Popov, Z. A. Piazza, W. L. Li, C. Romanescu, L. S. Wang and A. I. Boldyrev, *Acc. Chem. Res.,* 2014, **47,** 1349-1358.
11 N. G. Szwacki, A. Sadrzadeh and B. I. Yakobson, *Phys. Rev. Lett.,* 2007, **98,** 166804.
12 F. Li, P. Jin, D-E. Jiang, L. Wang, S. Zhang, J. Zhao and Z. Chen, *J. Chem. Phys.,* 2012, **136,** 074302.
13 S. De, A.Willand, M. Amsler, P. Pochet, L. Genovese and S. Goedecker, *Phys. Rev. Lett.,* 2011, **106,** 225502.
14 H. J. Zhai, Y. F. Zhao, W. L. Li, Q. Chen, H. Bai, H. S. Hu, Z. A. Piazza, W. J. Tian, H. G. Lu, Y. B. Wu, Y. W. Mu, G. F. Wei, Z. P. Liu, J. Li, S. D. Li and L. S. Wang, *Nat. Chem.,* 2014, **6,** 727–731.
15 Q. Chen, W. L. Li, Y. F. Zhao, S. Y. Zhang, H. S. Hu, H. Bai, H. R. Li, W. J. Tian, H. G. Lu, H. J. Zhai, S. D. Li, J. Li and L. S. Wang, *ACS Nano,* 2015, **9,** 754–760.
16 Q. Chen, S. Y. Zhang, H. Bai, W. J. Tian, T. Gao, H. R. Li, C. Q. Miao, Y. W. Mu, H. G. Lu, H. J. Zhai and S. D. Li, *Angew. Chem. Int. Ed.*, 2015, **54,** 8160–8164.
17 H. Bai, Q. Chen, H. J. Zhai and S. D. Li, *Angew. Chem. Int. Ed*., 2014, **54,** 941–945.
18 R. X. He and X. C. Zeng, *Chem. Comm.,* 2015, **51,** 3185–3188.
19. P. Schwerdtfeger, L. N. Wirz and J. Avery, *WIREs Comput. Mol. Sci.,* 2015, **5,** 96–145.
20 P. Jin, Q. Hou, C. Tang and Z. Chen, *Theor. Chem. Acc.*, 2015, **134,** 13–22.
21 G. Martínez-Guajardo, J. L. Cabellos, A. Díaz-Celaya, S. Pan, R. Islas, P. K. Chattaraj, T. Heine, and G. Merino, *Scientific Reports,* 2015, **5,** 11287.
22 H. Dong, T. Hou, S. T. Lee, and Y. Li, *Scientific Reports,* 2015, **5,** 09952.
23 Z. Yang, Y. L. Ji, G. Lan, L. C. Xu, X. Liu and B. Xu, *Solid State Commun.*, 2015, **217,** 38-42.
24 Q. Chen, T. Gao, W. J. Tian, H. Bai, S. Y. Zhang, H. R. Li, C. Q. Miao, Y. W. Mu, H. G. Lu, H. J. Zhai and S. D. Li, *Phys. Chem. Chem. Phys.,* 2015, **17,** 19690-19694.
25 J. R. Heath, S. C. O'Brien, Q. Zhang, Y. Liu, R. F. Curl, H. W. Kroto, F. K. Tittel and R. E. Smalley, *J. Am. Chem. Soc.,* 1985, **107,** 7779–7780.
26 Z. Wan, J. F. Christian and S. L. Anderson, *Phys. Rev. Lett.,* 1992, **69,** 1352–1355.
27 P. Weis, R. D. Beck, G. Bräuchle and M. M. Kappes, *J. Chem. Phys.,* 1994, **100,** 5684–5695.
28 Y. Kubozono, H. Maeda, Y. Takabayashi, K. Hiraoka, T. Nakai, S. Kashino, S. Emura, S. Ukita and T. Sogabe, *J. Am. Chem. Soc.,* 1996, **118,** 6998–6999.
29 L. S. Wang, J. M. Alford, Y. Chai, M. Diener, J. Zhang, S. M. McClure, T. Guo, G. E. Scuseria and R. E. Smalley, *Chem. Phys. Lett.,* 1993, **207,** 354–359.
30 M. Saunders, R. J. Cross, H. A. Jiménez-Vázquez, R. Shimshi and A. Khong, *Science,* 1996, **271,** 1693–1697.
31 T. A. Murphy, T. Pawlik, A. Weidinger, M. Höhne, R. Alcala and J. M. Spaeth, *Phys. Rev. Lett.,* 1996, **77,** 1075–1078.
32 J. Lu, X. W. Zhang and X. G. Zhao, *Chem. Phys. Lett.,* 1999, **312,** 85–90.
33 J. Lv, Y. Wang, L. Zhu and Y. Ma, *Nanascale,* 2014, **6**, 11692-11696.
34 T. B. Tai and M. T. Nguyen, *Nanoscale,* 2015, **7**, 3316-3317.
35 Q. L. Lu, Q. Q. Luo, Y. D. Li and S. G. Huang, *Phys. Chem. Chem. Phys.,* 2015, **17,** 20897-20902.
36 S. Goedecker, W. Hellmann and T. Lenosky, *Phys. Rev. Lett.,* 2005, **95,** 055501.
37. L. Wang, J. Zhao, F. Li, Z. Chen, *Chem. Phys. Lett.*, 2010, **501**, 16–19.
38 C. Adamo and V. Barone, *J. Chem. Phys.,* 1999, **110,** 6158–6170.
39 R. Krishnan, J. S. Binkley, R. Seeger and J. A. Pople, *J. Chem. Phys.,* 1980, **72,** 650–654.
40 M. J. Frisch, G. W. Trucks, H. B. Schlegel, G. E. Scuseria, M. A. Robb, J. R. Cheeseman, G. Scalmani, V. Barone, B. Mennucci and G. A. Petersson, *et al. Gaussian 09*, Revision B.01; Gaussian Inc., Wallingford, CT, 2010.
41 D. Feller, *J. Comput. Chem.,* 1996, **17,** 1571–1586.
42 K. L. Schuchardt, B. T. Didier, T. Elsethagen, L. Sun, V. Gurumoorthi, J. Chase, J. Li and T. L. Windus, *J. Chem. Inf. Model.,* 2007, **47,** 1045–1052.
43 J. Čížek, *Adv. Chem. Phys*., 1969, **14,** 35–89.
44 G. D. Purvis III and R. J. Bartlett, *J. Chem. Phys.,* 1982, **76,** 1910–1918.
45 K. Raghavachari, G. W. Trucks, J. A. Pople and M. Head-Gordon, *Chem. Phys. Lett.,* 1989, **157,** 479–483.
46 H. J. Werner, P. J. Knowles, G. Knizia, F. R. Manby, M. Schütz, P. Celani, T. Korona, R. Lindh, A. Mitrushenkov and G. Rauhut, *et al. MOLPRO*, version 2012.1.
47 J. V. Vondele, M. Krack, F. Mohamed, M. Parrinello, T. Chassaing and J. Hutter, *Comput. Phys. Commun.,* 2005, **167,** 103–128.
48 D. Yu. Zubarev and A. I. Boldyrev, *Phys. Chem. Chem. Phys.,* 2008, **10,** 5207–5217.

49 R. Bauernschmitt, R. Ahlrichs, *Chem. Phys. Lett.,* 1996, **256,** 454–464.
50 P. v. R. Schleyer and C. Maerker, *J. Am. Chem. Soc.,* 1996, **118,** 6317–6318.
51 G. J. Wang, M. F. Zhou, J. T. Goettel, G. J. Schrobilgen, J. Su, J. Li, T. Schlöder and S. Riedel, *Nature,* 2014, **514,** 475–477.
52 D. Ciuparu, R. F. Klie, Y. Zhu, and L. Pfefferle, *J. Phys. Chem.* B, 2004, **108,** 3967–3969.

TOC

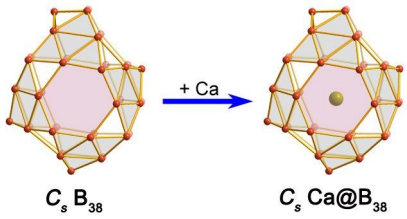

ΔE = –127.74 kcal/mol

We present the viability of an endohedral C_s Ca@B_{38} which contains a C_s B_{38}^{2-} borospherene cage composed of interwoven boron double chains with a σ+π double delocalization bonding pattern, extending the B_n^q (q = n–40) borospherene family from n = 39–42 to n = 38.